THE JOURNAL OF BIOLOGICAL CHEMISTRY VOL. 287, NO. 44, pp. 37119–37133, October 26, 2012
Published in the U.S.A.

Open Conformation of Ezrin Bound to Phosphatidylinositol 4,5-Bisphosphate and to F-actin Revealed by Neutron Scattering*[S]

Received for publication, May 14, 2012, and in revised form, August 22, 2012 Published, JBC Papers in Press, August 26, 2012, DOI 10.1074/jbc.M112.380972

Jayant James Jayasundar[‡], Jeong Ho Ju[‡], Lilin He[§¶], Dazhi Liu[¶], Flora Meilleur[¶‖], Jinkui Zhao[¶], David J. E. Callaway[‡], and Zimei Bu[‡1]**

*From the [‡]Department of Chemistry, City College of New York, New York, New York 10031, the [§]Center for Structural Molecular Biology and Chemical Sciences Division, Oak Ridge National Laboratory, Oak Ridge, Tennessee 37831, the [¶]Neutron Sciences Directorate, Oak Ridge National Laboratory, Oak Ridge, Tennessee 37831, the [‖]Department of Molecular and Structural Biochemistry, North Carolina State University, Raleigh, North Carolina 27695, and the **New York University School of Medicine, New York, New York 10016*

Background: The structure of activated ezrin is not known.
Results: We have determined the conformation of activated ezrin upon binding to PIP_2 and to F-actin.
Conclusion: Activated ezrin forms more extensive contacts with F-actin than generally depicted.
Significance: This study provides new insight into the mechanisms by which ezrin assembles signaling complexes at the membrane-cytoskeleton interface.

Ezrin is a member of the ezrin-radixin-moesin family (ERM) of adapter proteins that are localized at the interface between the cell membrane and the cortical actin cytoskeleton, and they regulate a variety of cellular functions. The structure representing a dormant and closed conformation of an ERM protein has previously been determined by x-ray crystallography. Here, using contrast variation small angle neutron scattering, we reveal the structural changes of the full-length ezrin upon binding to the signaling lipid phosphatidylinositol 4,5-bisphosphate (PIP_2) and to F-actin. Ezrin binding to F-actin requires the simultaneous binding of ezrin to PIP_2. Once bound to F-actin, the opened ezrin forms more extensive contacts with F-actin than generally depicted, suggesting a possible role of ezrin in regulating the interfacial structure and dynamics between the cell membrane and the underlying actin cytoskeleton. In addition, using gel filtration, we find that the conformational opening of ezrin in response to PIP_2 binding is cooperative, but the cooperativity is disrupted by a phospho-mimic mutation S249D in the 4.1-ezrin/radixin/moesin (FERM) domain of ezrin. Using surface plasmon resonance, we show that the S249D mutation weakens the binding affinity and changes the kinetics of 4.1-ERM to PIP_2 binding. The study provides the first structural view of the activated ezrin bound to PIP_2 and to F-actin.

Ezrin belongs to the ezrin-radixin-moesin (ERM)[2] family of membrane-cytoskeletal linker proteins. Members of the ERM family of proteins are structurally homologous and participate in regulating a variety of cellular functions such as tissue morphogenesis and intracellular trafficking of membrane receptors and transporters (1–8). Recent studies have identified ezrin as an essential element in cancer development and tumor metastasis (9–11). Despite their important functions, the mechanisms by which ERMs regulate cellular processes are not fully understood.

The ERM proteins are localized at the interface between cell membranes and the cortical F-actin cytoskeleton. Many important cellular functions of ERM proteins are due to the ability of ERMs to interact with both the cell membrane components and with the F-actin cytoskeleton. These cellular functions include regulating cell adhesion and migration (12, 13), assembling cell surface microvilli (14, 15), stabilizing actin-membrane attachment in retracting cell blebbing (16), forming immunological synapse (3), and virus entry into host cells and phagocytosis (17, 18). Ezrin and other ERMs participate in coordinated regulation of the cell membrane and the F-actin during these membrane-cytoskeleton-related events. Determining how ezrin undergoes conformational changes upon binding to the cell membrane component and to F-actin will provide important insight into the mechanisms by which ezrin and other ERMs regulate these membrane-cytoskeleton-related events.

Like other ERM proteins, ezrin contains an N-terminal 4.1-ezrin/radixin/moesin (FERM) domain of about 300 residues, a central helical linker region of about 170 residues, and a C-terminal ERM-associated domain (C-ERMAD) of about 80 residues (Fig. 1*A*). The FERM domain can bind directly with cell membrane lipid and transmembrane proteins such as the cell

* This work was supported, in whole or in part, by National Institutes of Health Grant 5R01HL086496 (to Z. B.).
[S] This article contains supplemental Figs. S1–S8, Tables S1 and S2, Equations S1 and S2 and an additional reference.
[1] To whom correspondence should be addressed: Dept. of Chemistry, City College of New York, Marshak Science Bldg., Rm. 1336, 160 Convent Ave., New York, NY 10031. E-mail: zbu@ccny.cuny.edu.
[2] The abbreviations used are: ERM, ezrin-radixin-moesin family of proteins; C-ERMAD, C-terminal ERM associated domain of ERM proteins; DHPC, 1,2-diheptanoyl-*sn*-glycero-3-phosphocholine; FERM, 4.1-ezrin/radixin/moesin domain; NHERF1, Na^+/H^+ exchanger regulatory factor 1; PIP_2, phosphatidylinositol 4,5-bisphosphate; SANS, small angle neutron scattering; SAXS, small angle x-ray scattering; Sfmoesin, moesin from *S. frugiperda*; SPR, surface plasmon resonance; [d]ezrin, deuterated ezrin; NSD, normalized spatial discrepancy.

adhesion molecules CD44, CD43, and ICAM-1/2/3 (19) or the G-protein couple receptor parathyroid hormone receptor (20, 21). The FERM domain can also interact with transmembrane proteins via the scaffolding protein Na^+/H^+ exchanger regulatory factor 1 or 2 (NHERF1 or NHERF2) (22, 23); FERM binds to the C-terminal domain of NHERF proteins tightly (22, 24), and the PDZ domains of the NHERF scaffolding proteins in turn bind to a number of transmembrane ion transport proteins and receptor complexes (25–28). The last 34 residues of C-ERMAD bind to F-actin (29–32). Because of the ability to interact with both the cell membrane components and the actin cytoskeleton, ERM proteins are membrane-cytoskeleton adapter proteins that form regulated signaling linkages between the assembled membrane signaling complexes and the actin cytoskeletal network.

The ERM proteins are regulated by an autoinhibitory mechanism, with the inactive protein being held in a closed and inactive conformation by head-to-tail-like intramolecular interactions (30, 33). X-ray crystallography studies reveal that the FERM domains of all ERM proteins adopt a conserved cloverleaf-like structure with three subdomains, F1, F2, and F3 (34, 35). In the closed ERMs, the central α-helical region folds back into an anti-parallel coiled coil (33). The C-ERMAD adopts an extended structure that binds extensively to the F2 and F3 subdomains, thus masking both the membrane-binding and the cytoskeleton-binding sites (36). Additionally, the crystal structure representing the full-length moesin from *Spodoptera frugiperda* (Sfmoesin) reveals that the N-terminal portion of the α-helical linker provides further protection to the FERM domain, further preventing FERM from binding to other proteins (33). Because of such tightly regulated intramolecular interactions, the inactive ERM proteins exhibit no binding to NHERF1 or to CD44 by the FERM domain or to F-actin by the C-ERMAD.

The ERM proteins are activated upon binding to the membrane signaling lipid phosphatidylinositol 4,5-bisphosphate (PIP_2) and/or by phosphorylation (37–39). Binding to PIP_2 is thought to release the head-to-tail intramolecular interaction in the ERMs. Phosphorylation at a conserved Thr in the C-ERMAD also contributes to ERM activation. This conserved residue is Thr-567 for ezrin, Thr-558 for moesin, and Thr-563 for radixin (40), which can be phosphorylated by a number of Ser/Thr kinases, including the Rho kinase (41), atypical protein kinase C (42), lymphocyte-oriented kinase (43), and MST4 (44). In cells, the phosphorylated ERMs are localized in the membrane extensions that are rich in actin (12, 45–47). Because this conserved Thr site is masked by the FERM domain in the dormant ERMs, PIP_2 binding is considered to cause conformational changes to make the C-terminal Thr site accessible to kinases for phosphorylation. It is proposed that PIP_2 binding and phosphorylation act sequentially in the activation of ezrin (48). A recent study shows that in the presence of PIP_2, ezrin binding to F-actin is enhanced by the T567D phosphomimic mutation (44).

We have determined the molecular conformation of activated ezrin in the PIP_2-bound and F-actin-bound states using contrast variation small angle neutron scattering (SANS). Similar to small angle x-ray scattering (SAXS), SANS determines the size, molecular mass, and shape of a protein in solution. Moreover, SANS has the capability of studying the structure of a multicomponent complex by contrast variation and deuterium labeling. By changing the D_2O concentration (or deuterium content) of a buffer solution, one varies the neutron scattering-length density contrast between the buffer background and a particular component in a complex. Contrast variation SANS can retrieve not only the overall shape but also the internal structure of a protein·lipid membrane, protein·DNA, or a multiprotein complex.

We find that the wild-type ezrin and phosphomimic mutants adopt a closed conformation in solution. PIP_2 binding is sufficient to induce the opening of ezrin. Additionally, using gel filtration, we find that the conformational opening of ezrin in response to PIP_2 binding is cooperative, but the cooperativity of conformational opening is abolished by a phospho-mimic mutation S249D in the FERM domain. Furthermore, ezrin binding to F-actin requires the simultaneous binding of ezrin to PIP_2. Once bound to F-actin, the opened ezrin forms more extensive contacts with F-actin than previously thought. This study provides the first view of how activated ezrin interacts with the membrane component PIP_2 and with F-actin.

EXPERIMENTAL PROCEDURES

Protein Expression and Purification—The human cDNA encoding the full-length ezrin was subcloned into the pET151/D-TOPO vector (Invitrogen). The T567D, S249D, and S249D/T567D mutants were generated with the QuikChange II site-directed mutagenesis kit (Agilent Technologies). The plasmids were transformed into Rosetta 2 (DE3) competent cells (EMD Biosciences). The bacterial cells were grown at 37 °C to an absorbance of 0.8 at 600 nm and were induced with 0.5 mM isopropyl β-D-1-thiogalactopyranoside for 2 h. The proteins were purified by a Ni^{2+}-chelating column and by gel filtration using a Superdex 200 10/300 GL column (GE Healthcare). The tag of the purified protein was cleaved by acetyl tobacco etch virus protease (Invitrogen). The cleaved tag and residual uncleaved proteins were removed by a Ni^{2+}-chelating column. The purity of the proteins is above 95% as estimated from SDS-PAGE (Fig. 1*B*).

For producing deuterated proteins, bacteria cells were grown at 37 °C in sterile D_2O M9 medium (D_2O 99.9%, Cambridge Isotope Laboratories) until the absorbance at 600 nm reached 0.7–0.8. The cells were induced with 0.25 mM isopropyl β-D-1-thiogalactopyranoside for 11–12 h. Purification of the deuterium-labeled protein was similar to that for the unlabeled protein. The nonexchangeable deuterium content of the purified deuterated proteins ranged from 0.63 to 0.67, as determined by matrix-assisted laser desorption time-of-flight mass spectrometry at the Columbia University Protein Core Facility. At such deuteration levels, the scattering length density of the deuterated protein approximately matched that of 100% D_2O buffer. To determine whether deuteration caused any conformational changes in ezrin, we compared the conformation of the hydrogenated ezrin and deuterated ezrin (^{d}ezrin) in buffer by SAXS and SANS (supplemental Fig. S1). The hydrogenated ezrin and ^{d}ezrin have identical R_g and D_{max} values (supplemental Table S1),

indicating that deuterium labeling does not cause conformational changes in the protein.

Lipid Micelle Preparation—The short chain lipid 1,2-diheptanoyl-*sn*-glycero-3-phosphocholine (DHPC) and PIP_2 ammonium salt from porcine brain, dissolved in 20:9:1 $CHCl_3$/MeOH/H_2O, were purchased from Avanti Polar Lipids, Inc. Before the experiments, the solvent from the PIP_2 solution was removed in a speed-vac for 1 h, and the dry PIP_2 film was dissolved in the buffer of 25 mM Tris (pH 7.5), 300 mM NaCl, 1 mM DTT.

F-actin Filament Preparation—Nonmuscle actin from a human platelet of higher than 99% purity was purchased from Cytoskeleton Inc. One milligram of lyophilized actin was resuspended by adding 100 μl of 20 mM Tris-HCl (pH 7.5), 0.2 mM $CaCl_2$, 0.2 mM ATP, and 0.2 mM DTT. The protein concentration was determined by measuring the absorbance at 280 nm, using the molar extinction coefficient $\epsilon = 42{,}680\ M^{-1}cm^{-1}$ and a molecular mass = 41.7378 kDa. A 10× F-actin polymerization buffer of 500 mM KCl, 20 mM $MgCl_2$, and 10 mM ATP was added to achieve a final concentration of 1× to initiate actin polymerization. Actin was allowed to polymerize at room temperature for 1 h.

Surface Plasmon Resonance Experiments—SPR experiments were performed on a Biacore X100 (GE Healthcare). For studying the binding of FERM or FERM(S249D) to PIP_2, purified FERM and FERM(S249D) were dialyzed overnight in SPR binding buffer, containing 10 mM Hepes (pH 7.5), 300 mM NaCl, 3 mM EDTA. An L1 chip was coated with 0.4 mM PIP_2 + 16 mM DHPC to a response unit of 424.9. The analyte, FERM, or FERM(S249D) was injected onto the chip at a flow rate of 30 μl/min at 10 °C. The sensor chip was regenerated by passing 20 mM NaOH after each analyte injection. The sensorgrams were fit with a 1:1 kinetic binding model with the manufacturer's supplied program to obtain the rate constant k_{on} and k_{off}, as well as the dissociation constant K_d.

Gel Filtration Analysis of Conformational Opening upon Binding to Lipid—A super Superdex 200 10/300 GL gel filtration column was used to analyze the conformational opening of ezrin and mutants in DHPC and PIP_2. The buffer used for these gel filtration analyses is 25 mM Tris (pH 7.5), 300 mM NaCl, 0.5 mM DTT, and 0.1 mM EDTA. Before the experiment, 9.9 μM ezrin or a mutant and 50.5 mM DHPC were incubated with PIP_2 at different molar ratios for 1 h. The experiments were repeated with a protein concentration of 6.2 μM and PIP_2 at different molar ratios of incubation. The gel filtration peaks representing the closed, partially open, or open conformation of ezrin were integrated using Origin 8.1 (OriginLab). At each PIP_2 concentration, the fraction of conformational opening (F_o) of ezrin or ezrin(T567D) can be calculated by integrating the peak areas of the closed (A_{closed}), partially opened ($A_{partially\ open}$), and fully opened (A_{open}) conformations in the gel filtration chromatograms as shown in Equation 1,

$$F_o = \frac{A_{open}}{A_{closed} + A_{partially\ open} + A_{open}} \quad \text{(Eq. 1)}$$

The F_o *versus* PIP_2 concentration data were either fit with a sigmoidal function $F_o = B_{max}\,(L^n)/(K^n + L^n)$, where L is the ligand concentration, K is the mid-point of transition, and B_{max} the top asymptote.

Solution Small Angle X-ray Scattering—SAXS experiments were performed with an in-house apparatus, utilizing a MicroMaxTM-007 HF Microfocus rotating anode generator as the x-ray source (Rigaku/MSC). In this study, a $0.014 < Q < 0.32$ $Å^{-1}$ range was covered, where $Q = 4\pi\sin\theta/\lambda$ is the magnitude of the scattering vector; θ is half the scattering angle, and λ is the wavelength of the x-ray. Details about SAXS data reduction and analysis have been described previously (49–51).

Solution Small Angle Neutron Scattering—SANS experiments were performed at the Bio-SANS (CG3) at the High Flux Isotope Reactor and at the EQ_SANS at the Spallation Neutron Source (52), Oak Ridge National Laboratory. At the Bio-SANS, the neutron wavelength, λ, was 6 Å, with a wavelength spread, $\Delta\lambda/\lambda$, of 0.14 obtained with a velocity selector. Scattered neutrons were detected with a $1 \times 1\ m^2$ helium-filled two-dimensional position sensitive detector with 192×192 pixels. Two sample-to-detector distances, 8 and 1.7 m, were used to cover a Q range between $Q_{min} = 0.008\ Å^{-1}$ and $Q_{max} = 0.4\ Å^{-1}$. The data acquisition time from the samples varied from ~20 min to 4 h at each detector position to ensure sufficient data statistics. The two-dimensional raw counts were corrected for nonuniform detector response and electronic dark current, which represents the ambient radiation background and electronic noise and azimuthally averaged to produce a one-dimensional profile $I(Q)$. The data processing procedure for EQ-SANS has been described previously (53). At EQ-SANS, the Q range covered is between $Q_{min} = 0.008\ Å^{-1}$ to $Q_{max} = 0.5\ Å^{-1}$. Data were placed on an absolute scale in units of cm^{-1} through the use of pre-calibrated secondary standards (54).

Before SANS experiments, the protein, protein·lipid, and protein·lipid·F-actin complexes were dialyzed against buffer containing the desired D_2O volume fraction for two times, each time for about 8 h. The buffer used for SANS experiments contains 25 mM Tris (pH 7.5), 300 mM NaCl, 1 mM DTT. Protein concentrations in buffer and lipid were measured by UV absorption spectroscopy at 280 nm, using the calculated extinction coefficients based on the amino acid sequence of the recombinant proteins. For ezrin in complex with both the lipid and F-actin, the concentrations were estimated based on the concentrations of the stock solution. The protein concentrations used in the SANS experiments range between 1.0 and 1.85 mg/ml. At these protein concentrations, the inter-molecular interactions are negligible (see supplemental Figs. S2 and S3). The SANS buffer background at each D_2O volume fraction was taken from the dialysis buffer. The sample cells used for SANS experiments are 1-mm quartz cuvettes.

SANS Data Analysis and Three-dimenional Shape Reconstruction—The length distribution function $P(r)$, radius of gyration R_g, the forward scattering intensity $I(0)$, and the maximum dimension D_{max} were calculated from the scattering data using the program GNOM (55). R_g and $I(0)$ can also be obtained from Guinier fitting (see supplemental Table S1). The three-dimenional "dummy bead" coordinates were generated using the program DAMMIN (56). Multiple calculations were performed using DAMMIN, and the generated 10 structures were averaged and filtered using the program DAMAVER and

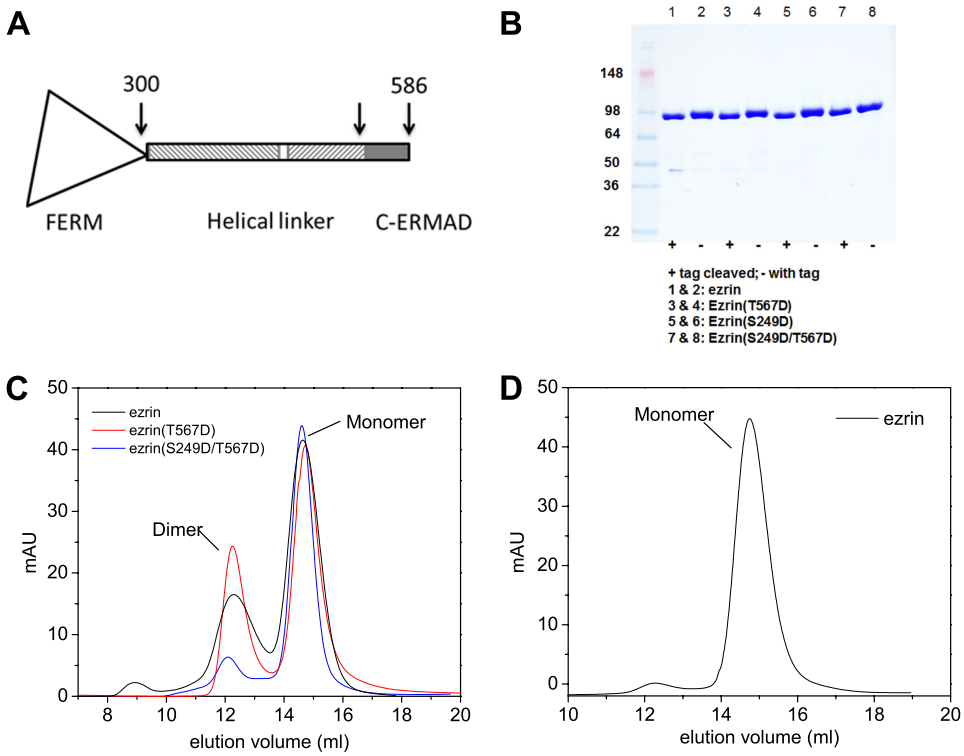

FIGURE 1. *A,* amino acid sequence and domain organization of ezrin. *B,* SDS-PAGE of purified ezrin and ezrin mutants before and after tobacco etch virus cleavage of the His_6-V5 epitope tag. *C,* gel filtration chromatograms of the monomer and dimer fractions of ezrin, ezrin(T567D), and ezrin(S294D/T567D). *D,* re-run gel filtration of the monomer fraction of ezrin gives mostly monomer on the chromatogram, suggesting that the monomer fraction does not quickly equilibrate with the dimer fraction on the time scale of the experiment. *mAU*, milli-absorption unit.

DAMFILT (57). The normalized spatial discrepancy (NSD) value, which is a measure of reproducibility of the generated three-dimenional shape, is given in the figure legends. The three-dimenional density map was generated from the averaged coordinates using the program Situs (58). The fitting and docking of the high resolution structure to the density map were performed using Situs or UCS Chimera (59).

The scattering from an F-actin or a protein·F-actin complex can be considered as the scattering from a long rod (60, 61) as shown in Equation 2,

$$QI(Q) = 2\pi \int_0^\infty p_c(r) J_o(Qr) dr \qquad \text{(Eq. 2)}$$

with $P_c(r)$ the cross-section length distribution function, and $J_o(QR)$ the zero-order Bessel function. The cross-section forward scattering intensity $I_c(0)$ is related to the mass per unit length of the complex M_L (see supplemental material) (62). The cross-section length distribution function of the filament, $P_c(r)$, was obtained using the program GNOM (56), which also gives the cross-section radius of gyration R_c, and the cross-section maximum dimension $D_{max,c}$. The scattering Q range of $0.02 < Q < 0.20$ Å^{-1} was used to calculate $P_c(r)$.

RESULTS

Closed and Autoinhibited Conformation of Ezrin and Phospho-mimic Mutants in Solution—Previous biochemical studies have shown that phosphorylation at Thr-567 in the C-ERMAD of ezrin contributes to ezrin activation (12, 45–47). A Thr → Asp or Ser → Asp mutation is often employed to mimic the negative electrostatic charges of a phosphorylated Thr or Ser (47, 63, 64). Recently, we have identified a new conserved phosphorylation site Ser-249 in the FERM domain of ezrin, and we have found that cells expressing the phospho-mimic ezrin(S249D) and ezrin(S249D/T567D) show significantly weakened cell-cell adhesion, as well as altered subcellular localizations of ezrin. We have characterized the oligomer states of the full-length wild-type ezrin and the phospho-mimic mutants, ezrin(T567D) and ezrin(S249D/T567D), using gel filtration and static light scattering.

For both ezrin and ezrin(T567D), the gel filtration chromatograms show two peak fractions, one at elution volume 12.3 ml and the other at 14.7 ml (Fig. 1*B*). Static light scattering indicates that the fraction at elution volume 12.3 ml is a dimer, although the fraction at 14.7 ml is a monomer (supplemental Fig. S3). The dimer fraction of ezrin(S249D/T567D) is significantly reduced compared with that of ezrin or ezrin(T567D) (Fig. 1*C*). Additionally, the monomer fraction of ezrin or ezrin(T567D) does not convert to a dimer fraction after gel filtration separation (Fig. 1*D*), and the dimer fraction decreases after storing the proteins on ice for several days.

We then performed solution SAXS experiments on the monomer and the dimer fractions of ezrin (supplemental Fig. S1). The radius of gyration (R_g) and the maximum dimension (D_{max}) of the monomeric ezrin from SAXS are listed in Table 1. For the dimer fraction of ezrin, SAXS yields similar R_g and D_{max} values as the monomer fraction, suggesting that ezrin has converted to the folded monomer conformation during the exper-

TABLE 1

Comparing R_g, D_{max}, and $I(0)/c$ of ^{d}ezrin* and mutants in buffer, PIP_2-bound, and F-actin-bound states

Static light scattering experiments (see supplemental Fig. S3), which measure the absolute molecular mass, show that the fraction of ezrin eluted at 14.6 ml in the Superdex 200 10/300 GL column is monomeric. The parameters listed here are from $P(r)$ function calculations. See supplemental Table S1 for R_g and $I(0)$ obtained from Guinier fit.

	In 20% D_2O buffer			In 2.5 mM PIP_2 in 20% D_2O			Bound to PIP_2 and to F-actin in 40% D_2O		
	R_g	D_{max}	$I(0)_{abs}/c$	R_g	D_{max}	$I(0)_{abs}/c$	R_g	D_{max}	$I(0)_{abs}/c$
	Å	Å	$cm^2\ mg^{-1}$	Å	Å	$cm^2\ mg^{-1}$	Å	Å	$cm^2\ mg^{-1}$
Ezrin[a]	41.2 ± 0.3	140							
^{d}Ezrin	40.7 ± 0.5	140	0.31 ± 0.01	67.4 ± 1.2	240	0.28 ± 0.01			
^{d}Ezrin(T567D)	41.0 ± 0.8	140	0.30 ± 0.01	68.0 ± 1.0	240	0.33 ± 0.01	95.2 ± 0.9	300	0.80 ± 0.05
^{d}Ezrin(S249D)	41.4 ± 0.7	140	0.32 ± 0.01						
^{d}Ezrin(S249D/T567D)	42.0 ± 0.9	150	0.31 ± 0.01						

[a] Data are from SAXS measurements.

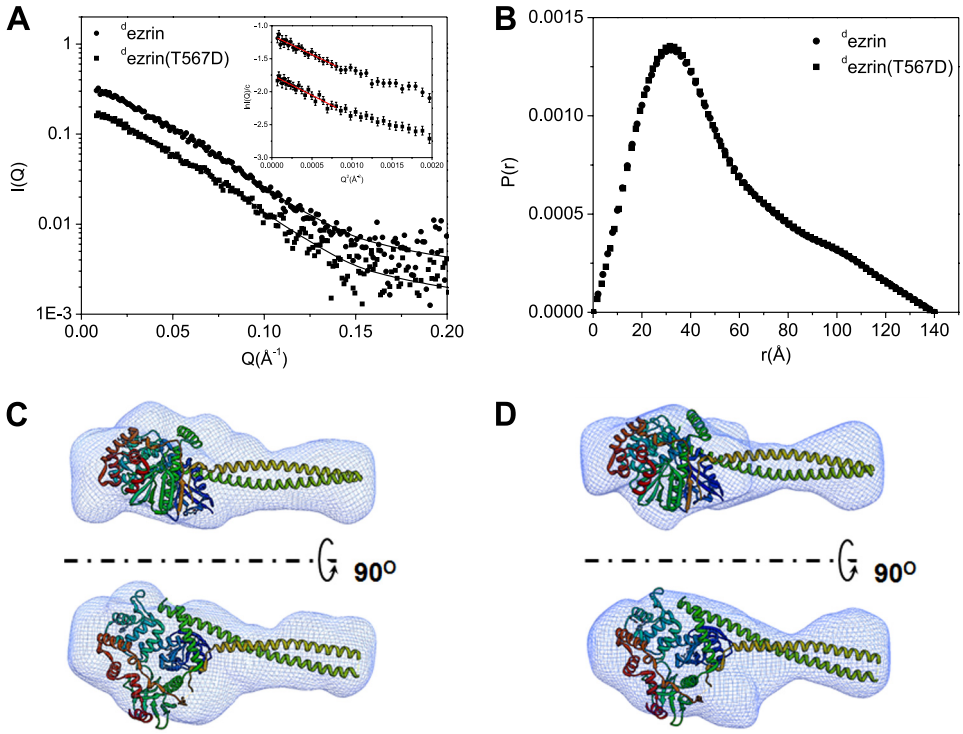

FIGURE 2. **Comparing the structures of ezrin and phospho-mimetic ezrin(T567D) in solution using SANS.** *A,* SANS $I(Q)$ of ^{d}ezrin at 1.75 mg/ml and ^{d}ezrin(T567D) at 1.57 mg/ml. $I(Q)$ values are scaled to show the different scattering curves. The lines are fit to the experimental data when *ab initio* reconstructs the three-dimenional shapes shown in *C* and *D*. The χ^2 values for the fit are 0.356 and 0.377 for ^{d}ezrin and ^{d}ezrin(T567D), respectively. The Guinier plots and fits are shown in the *inset*. *B, P(r)* functions of ^{d}ezrin and ^{d}ezrin(T567D). *C* and *D, ab initio* reconstructed three-dimenional envelopes of ^{d}ezrin and ^{d}ezrin(T567D) are docked with the crystal structure of Sfmoesin (Protein Data Bank code 2I1K). The models are generated by averaging 10 models generated by DAMMIN. The largest NSD value (57) with ^{d}ezrin three-dimenional shape is 0.606 and 0.559 for ^{d}ezrin(T567D).

iment. We thus focus on analyzing the monomer fraction of ezrin in the SANS experiments.

Fig. 2 shows the SANS results from deuterated wild-type ezrin (^{d}ezrin) and deuterated ezrin(T567D) (^{d}ezrin(T567D)) in solution. Overall, R_g, D_{max}, and $P(r)$ values of ^{d}ezrin are identical to those of ^{d}ezrin(T56D) (Table 1 and Fig. 2, *A* and *B*). Fig. 2*C* shows the three-dimenional molecular envelopes of ^{d}ezrin and ^{d}ezrin(T567D), *ab initio* reconstructed from SANS. For comparison, the reconstructed three-dimenional maps are docked to the crystal structure of Sfmoesin (Protein Data Bank code 2I1K) that represents the closed and auto-inhibited conformation of an intact monomeric ERM protein (Fig. 2*C*) (33). The crystal structure of the autoinhibited form of Sfmoesin has a central helical linker composed of two helices folded into antiparallel coiled-coil conformation. The comparison indicates that both ^{d}ezrin and ^{d}ezrin(T567D) adopt a closed conformation in solution, and the phospho-mimetic ^{d}ezrin(T567D) does not have apparent conformational changes when compared with the wild-type protein.

Fig. 3 compares the SANS results from the deuterated ^{d}ezrin, ^{d}ezrin(S249D), and the double mutant ^{d}ezrin(S249D/T567D) in solution. Overall, ^{d}ezrin(S249D) and ^{d}ezrin(S249D/T567D) also adopt a closed form as ^{d}ezrin and ^{d}ezrin(T567D) (Fig. 3*B*). However, the $P(r)$ functions of ^{d}ezrin(S249D) and ^{d}ezrin(S249D/T567D) show a more pronounced shoulder at r 32 ≈90 Å, and R_g and D_{max} values of ^{d}ezrin(S249D/T567D) are slightly larger than the wild-type protein (Fig. 3*B* and Table 1).

Using SPR, we have also estimated the fraction of ezrin, ezrin(T567D), ezrin(S249D), and ezrin(S249D/T567D) that is capable of binding to target protein NHERF1. Previous biochemical and structural studies have shown that the conserved NHERF1-binding site is located in the F3 subdomain of FERM,

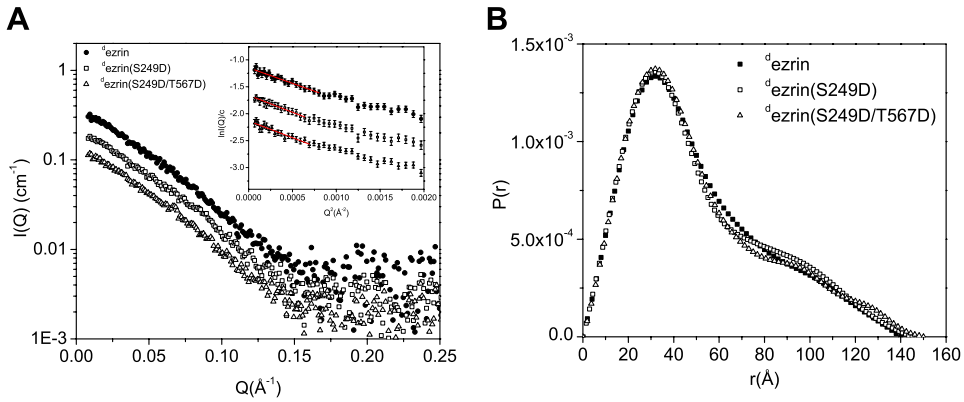

FIGURE 3. **Comparing the structures of ezrin, phospho-mimics ezrin(S249D), and ezrin(S249D/T567D) in solution using SANS.** *A,* SANS *I*(*Q*) of ^{d}ezrin at 1.75 mg/ml, ^{d}ezrin(S249D) at 1.85 mg/ml, and ^{d}ezrin(S249D/T567D) at 1.84 mg/ml. *I*(*Q*) values are scaled to show the different scattering curves. *B, P*(*r*) functions of ^{d}ezrin, ^{d}ezrin(S249D), and ^{d}ezrin(S249D/T567D).

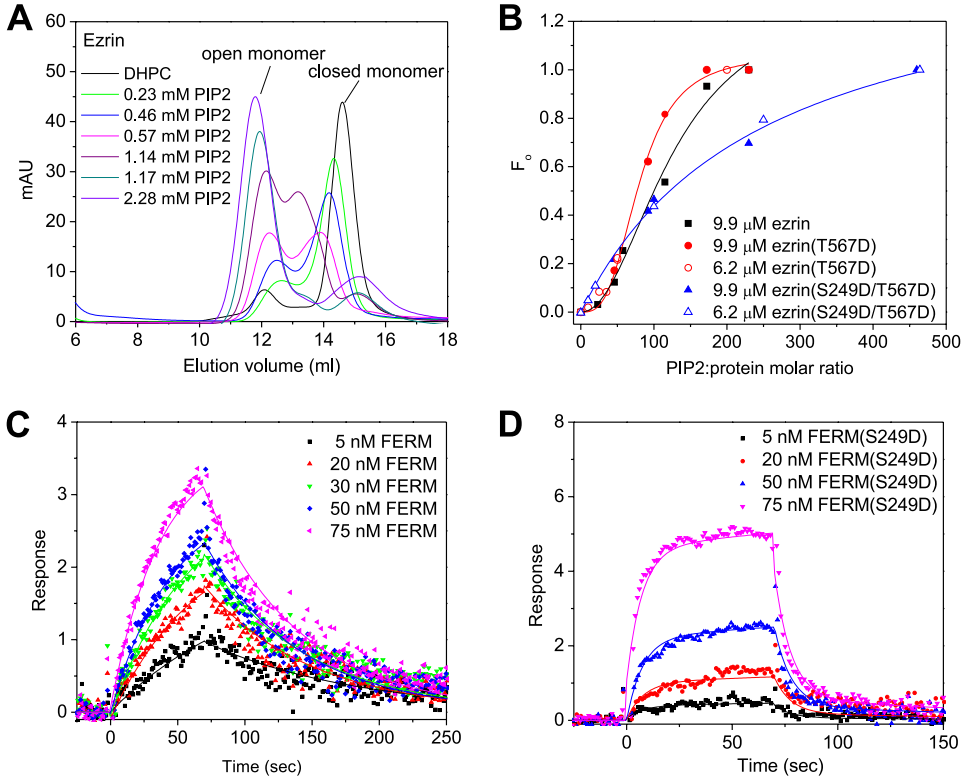

FIGURE 4. **Phospho-mimic S249D mutation affects ezrin binding to PIP_2 and the cooperativity of ezrin opening in response to PIP_2 binding.** *A,* gel filtration analysis of ezrin conformational changes in response to PIP_2 binding. The incubations contain 9.9 μM proteins, 50.5 mM DHPC, and PIP_2 at various concentrations. *mAU,* milli-absorption unit. *B,* comparing F_o *versus* the molar ratios of PIP_2 to ezrin, ezrin(T567D), or ezrin(S249D/T567D) suggests that S249D affects the cooperativity of ezrin activation in response to PIP_2 binding. *C,* SPR sensorgrams of FERM to PIP_2 binding. *D,* SPR sensorgrams of FERM(249D) to PIP_2 binding.

which is masked by C-ERMAD in the closed form of full-length ezrin (33, 65, 66). Using the monomer fraction from gel filtration, we find that an insignificant 0.4% fraction of the wild-type ezrin is capable of binding to NHERF1, whereas 16.2% ezrin(T567D), 18.3% ezrin(S249D), and about 27% ezrin(S249D/T567D) are capable of binding NHERF1 (supplemental Table S2).

The SANS and SPR results thus confirm that in the wild-type ezrin, FERM is tightly auto-regulated or masked by C-ERMAD. The results also show that although the phospho-mimic mutants are largely folded, they are more dynamic than the wild-type protein because a considerable fraction of the mutants is capable of binding to NHERF1 (supplemental Table S2). It is likely that inter-domain motions between the FERM and the C-ERMAD domain are activated in the phospho-mimic mutants, so that a fraction of the mutants can sample the conformational states that are capable of binding to NHERF1.

Phospho-mimetic Ezrin(S249D) Mutation Abolishes the Cooperativity of Conformational Opening of Ezrin in Response to PIP_2 Binding—We have performed a gel filtration analysis of the binding of ezrin, ezrin(T567D), or ezrin(S249D/T567D) to the short chain phospholipid DHPC and to the signaling lipid PIP_2. After 9.9 μM ezrin or ezrin(T567D) is incubated with 50.5 mM DHPC alone for an hour, the dimer fraction eluting at 12.3 ml disappears, and only the monomer fraction elutes at 14.7 ml in the gel filtration chromatogram (Fig. 4*A* and supplemental Fig. S4). DHPC thus can disrupt the dimer fraction of ezrin or

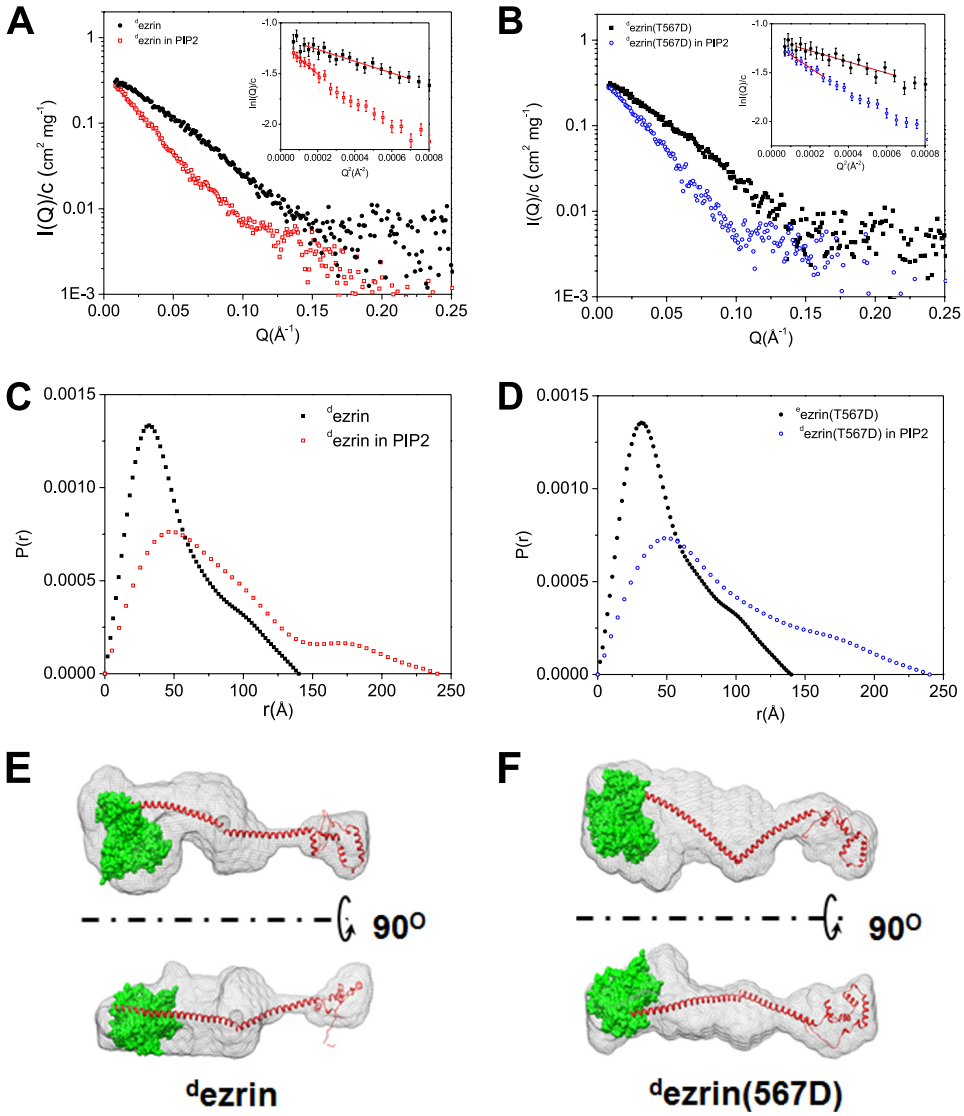

FIGURE 5. **Conformational changes of ^{d}ezrin and ^{d}ezrin(T567D) upon binding to PIP_2 revealed by SANS performed in 20% D^2O, at the contrast matching point of PIP_2.** *A*, comparison of *I*(*Q*)/*c* of ^{d}ezrin at 1.75 mg/ml in solution and ^{d}ezrin at 2.3 mg/ml in 4.6 mM PIP_2. *B*, comparison of *I*(*Q*) of ^{d}ezrin(T567D) at 1.57 mg/ml in solution and ^{d}ezrin(T567D) at 1.41 mg/ml in 4.6 mM PIP_2. *B* and *C*, the scattering intensities are on absolute scales and are normalized by protein concentration *c*. *C*, comparison of *P*(*r*) of ^{d}ezrin in solution and in PIP_2. *D*, comparison of *P*(*r*) of ^{d}ezrin(T567D) in solution and in PIP_2. *E*, three-dimenional shapes of opened ^{d}ezrin in PIP_2 reconstructed from SANS. The largest NSD value is 0.673 from the 10 models used to generated the averaged structure. *F*, three-dimenional shape of opened ^{d}ezrin(T567D) in PIP_2 reconstructed from SANS. The model is generated by averaging 10 models generated from DAMMIN. The largest NSD value is 0.610 from the 10 models used to generated the averaged model.

ezrin(T567D) but cannot open the closed autoinhibited form of ezrin or ezrin(T567D). Because the elution volume of the monomer fraction remains unchanged in the presence of DHPC as compared with that in buffer (Fig. 4*A* and supplemental Fig. S1), DHPC does not bind to ezrin or to ezrin(T567D) significantly to affect the size of the eluted protein.

When PIP_2 is incubated with ezrin in the presence of DHPC, the gel filtration chromatogram starts to show a fraction that elutes at 12.9 ml (Fig. 4*A*). Our contrast-matching SANS shows that PIP_2 binding induces large conformational changes but does not alter the oligomeric states of ezrin (see Fig. 5*A* and Table 1). The peak fraction at a 12.9-ml elution volume thus indicates significant conformational changes in the PIP_2-bound ezrin (Fig. 4*A*). For ezrin or ezrin(T567D), the peak height of the opened conformation fraction increases with increasing PIP_2 concentrations until the PIP_2/protein molar ratio reaches 230 (Fig. 4*A* and supplemental Fig. S4). In addition, with increasing PIP_2 concentrations, the "closed" form of ezrin also becomes more expanded in the gel filtration chromatogram (Fig. 4*A*), suggesting the existence of intermediate states. These intermediate states may be either PIP_2-bound closed monomer or partially open monomer. At the PIP_2/protein molar ratio, the ezrin·PIP_2 complex only elutes as an open conformation, suggesting that ezrin is fully opened. The lipid·protein complexes preclude light scattering from determining the size and molecular mass of the protein. These results indicate that PIP_2 binds to ezrin or ezrin(T567D) and causes conformational changes in ezrin or ezrin(T567D).

The fraction of conformational opening (F_o) of ezrin or ezrin(T567D) in response to PIP_2 binding can be calculated from the peak areas of the opened and closed forms of the protein (see "Experimental Procedures"). In Fig. 4*B*, F_o of

TABLE 2
Summary of cross-section information of F-actin and ^{d}ezrin(T567D)/F-actin complex obtained from SANS experiments

	R_c	$D_{c,\max}$	$I_c(0)_{abs}/c$	M_L
	Å	*Å*	$cm^2\,Å^{-1}\,g^{-1}$	$g\,mol^{-1}Å^{-1}$
F-actin in 80% D_2O	22.5 ± 0.9	70	0.728	1637.4
F-actin in 100% D_2O	23.2 ± 0.6	75	1.671	1614.4
PIP_2/^{d}ezrin(T567D)/F-actin	32.8 ± 0.1[a]	130		3124.8[b]
F-actin model	24.74	70		
PIP_2/^{d}ezrin(T567D)/F-actin in 100% D_2O	23.5 ± 0.2	70		

[a] Data were obtained in 0% D_2O from Fig. 7*B*.
[b] Data were obtained from the slope of Fig. 7*C*.

ezrin(T567D) shows a sigmoidal response to PIP_2 concentration with a mid-point of transition of 80.0 ± 3.5 and a Hill coefficient of 3.1 ± 0.4 (Fig. 4*B*). For the wild-type ezrin, F_o also shows a sigmoidal response to PIP_2 concentration with a mid-point of transition 136 ± 40 mM and a Hill coefficient of 2.1 ± 0.5 (Fig. 4*B*). These analyses illustrate the cooperative opening of the conformation of ezrin or ezrin(T567D) in response to PIP_2 binding. The Hill coefficients of PIP_2 binding to the wild-type of ezrin or to ezrin(T567D) suggest that more than one PIP_2 molecule is required in the process of opening and activating ezrin.

Ezrin(S249D/T567D) shows quite a different PIP_2 binding and conformational opening behavior as compared with that of ezrin or ezrin(T567D) (Fig. 4*B* and supplemental Fig. S3). The F_o curve is noncooperative, with a Hill coefficient of 1.05 ± 0.07 (Fig. 4*B*), and a mid-point of transition of 227.6 ± 39. The ezrin(249D/T567D) mutant has abolished the cooperativity of conformational opening in response to PIP_2 binding, and the opening of the ezrin(S249D/T567D) also requires a higher PIP_2 concentration. Comparing the F_o value of the wild-type ezrin, ezrin(T567D), and ezrin(S249D/T567D) indicates that the S249D mutant affects the PIP_2 binding behavior.

Although F_o is an indication of the conformational transition, the mid-point of F_o is not necessarily the same as the dissociation constant K_d of ezrin to PIP_2 binding. We have thus performed SPR analysis of the affinity and kinetics of PIP_2 binding to FERM and FERM(S249D) (Fig. 4, *C* and *D*, and Table 2). SPR shows that PIP_2 has a considerably higher affinity for FERM with K_d = 77.1 nM (protein concentration) than for FERM(S249D) with K_d = 1207 nM. Moreover, the kinetic processes of PIP_2 binding to FERM and to FERM(S249D) are also different (Fig. 4, *C* and *D,* and Table 3). The k_{on} values of FERM to PIP_2 binding is about two times slower than FERM(S249D), and k_{off} indicates that FERM(S249D) dissociates from PIP_2 about 10 times faster than FERM. The FERM(S249D) mutation thus has significantly altered both the PIP_2 binding affinity and kinetics, suggesting that FERM(S249D) is less competent to interact with PIP_2 than the wild-type FERM.

Open Conformation of Ezrin Bound to PIP$_2$—We have performed contrast-matching SANS experiment to determine the conformational changes in ^{d}ezrin and ^{d}ezrin(T567D) upon binding to PIP_2. The scattering of neutrons from PIP_2 becomes "invisible" in 20% D_2O because the neutron scattering length density of the buffer matches that of the lipid. At the contrast-matching point of the PIP_2 lipid, SANS determines the conformational changes of the deuterated proteins that have sufficient coherent neutron scattering without the interference scattering from the lipid. The concept and applications of contrast-matching small angle scattering have been described elsewhere (27, 50, 51, 60, 62, 67, 68).

TABLE 3
Comparing the kinetics and affinity of PIP_2 binding to FERM and to FERM(S249D) using SPR

	k_{on}	k_{off}	K_d
	1/MS	*1/s*	*nM*
FERM	2.140×10^5	0.0165	77.1
FERM(S249D)	1.453×10^5	0.1754	1207

Fig. 5 presents the SANS results from 20.1 μM ^{d}ezrin and ^{d}ezrin(T567D) in 20% D_2O buffer and in 4.6 mM PIP_2 20% D_2O buffer. At such a PIP_2/protein molar ratio, our gel filtration experiments have shown that both ezrin and ezrin(T567D) become fully opened. The neutron scattering intensities shown in Fig. 5, *A* and *B* are on absolute scales and are normalized by the protein concentration *c*. The forward scattering intensity $I(0)/c$, which is proportional to the protein molecular mass, of ^{d}ezrin in 20% D_2O buffer is nearly identical to that in PIP_2 solution (Fig. 5*A* and Table 1). Similarly, $I(0)/c$ of ^{d}ezrin(T567D) in 20% D_2O buffer is also the same as that in PIP_2 (Fig. 5*B* and Table 1). Using both static light scattering and SANS, we have confirmed the molecular mass of the monomer fraction of ezrin and ezrin(T567D) (Fig. 2 and supplemental Fig. S4). Comparing $I(0)/c$ thus indicates that ^{d}ezrin and ^{d}ezrin(T567D) remain as monomers in PIP_2 solution, and PIP_2 does not cause oligomer state changes in ezrin. Nevertheless, in PIP_2, the size of ^{d}ezrin or ^{d}ezrin(T567D) increases significantly when comparing with their respective closed forms in solution. The size of ^{d}ezrin expands to R_g = 67.4 ± 1.2 Å and D_{max} = 240 ± 5 Å and that of ^{d}ezrin(T567D) has also increased, with R_g = 68.0 ± 1.0 Å and D_{max} = 240 ± 5 Å (Fig. 5, *C* and *D*, and Table 1). Thus, contrast-matching SANS reveals the monomeric and open structures of ^{d}ezrin and ^{d}ezrin(T567D).

Fig. 5, *E* and *F,* gives the three-dimenional shapes of open ^{d}ezrin and ^{d}ezrin(T567D) in PIP_2 *ab initio* reconstructed from SANS using the program DAMMIN (56). The docked atomic model is taken from the crystal structure of Sfmoesin (33), but the two antiparallel central helices are unwind and one of the helices rotates about 120–180°. In the three-dimenional map, the center-of-mass distance between FERM and the C-ERMAD is about 180 Å, which agrees with a previous biophysical finding that the moesin α-helical coiled coil becomes an unfolded rod-like structure (69). In addition, the three-dimenional map shows extra density in the central hinge region between the two central helical halves. This is likely due to swivel-like motions between the FERM and

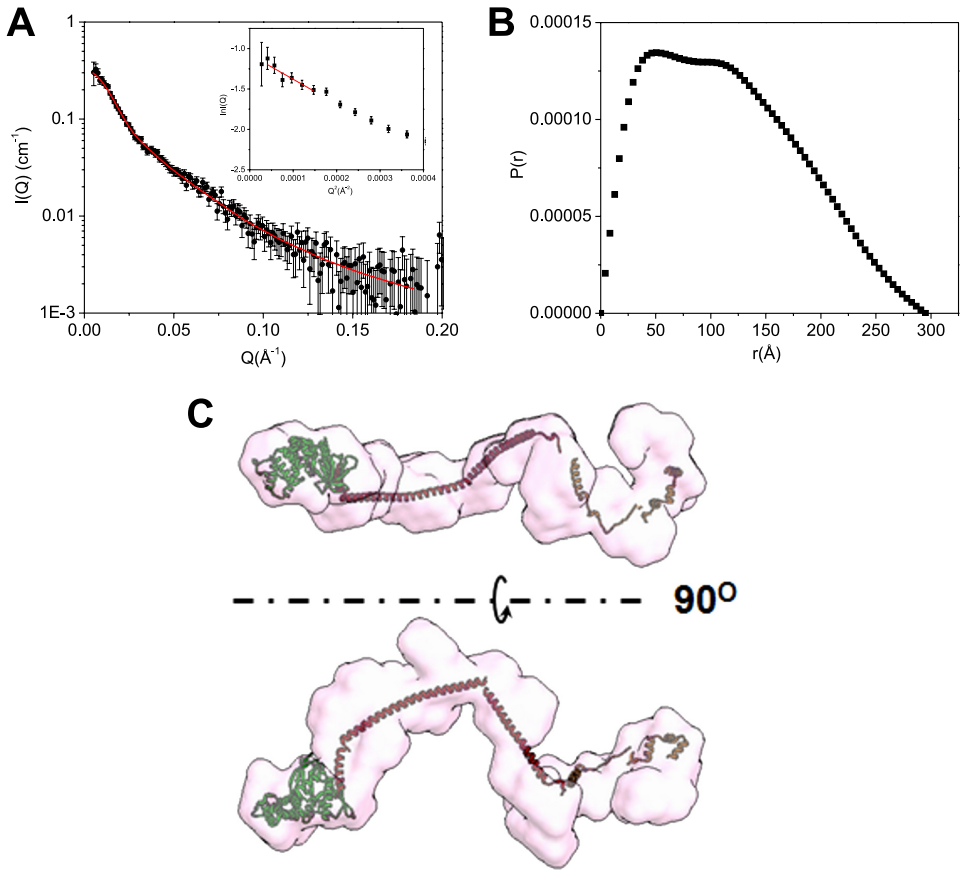

FIGURE 6. **Conformational changes of ^{d}ezrin(T567D) upon binding to PIP_2 and to F-actin.** *A, I(Q) versus Q* plot of PIP_2·^{d}ezrin(T567D)·F-actin in 40% D_2O at the contrast matching point of F-actin. The Guinier plot is shown in the *inset*. The concentrations of ^{d}ezrin(T567D), PIP_2, and F-actin are 0.41 mg/ml (5.8 μM), 58 μM, and 1.79 mg/ml (42.9 μM), respectively. *B, P(r)* function of ^{d}ezrin(T567D)·PIP·PIP_2 in complex with F-actin reconstructed from SANS. The largest NSD value is 1.054 from the 10 models used to generated the averaged model. *C,* the three-dimensional shape of the open ^{d}ezrin(T567D) in the PIP_2·^{d}ezrin(T567D)·F-actin complex reconstructed from SANS data in 40% D_2O buffer.

C-ERMAD about the hinge connecting the two halves of the central helices. Previously, we have shown the highly fluctuating region of a protein tends to be overestimated by the *ab initio* reconstruction method (70).

Open Conformation of Ezrin Bound to F-actin—We have first used SANS to determine the conditions of ezrin binding to F-actin. In 40% D_2O buffer, which is the contrast-matching point of the hydrogenated F-actin, SANS detects structural changes in the deuterated protein. When 13.7 μM ^{d}ezrin(S249D/T567D) is incubated with 68.3 μM F-actin, the size and $P(r)$ of the ^{d}ezrin(S249D/T567D) are similar to those of the closed ezrin in buffer (supplemental Fig. S5, *A* and *B*). The closed ezrin alone thus does not bind to F-actin. However, when ^{d}ezrin(T567D) is incubated with both PIP_2 and F-actin in 40% D_2O buffer, SANS detects significant conformational changes. R_g increased to 93.2 ± 1.7 Å and D_{max} to 300 Å (Fig. 6, *A* and *B*, and Table 1). Considering that 40% D_2O is close to the contrast-matching point of PIP_2, the deuterated ^{d}ezrin(T567D) dominates the scattering, and the detected size changes in 40% D_2O mainly reflect the conformational changes of ^{d}ezrin(T567D). Fig. 6*C* presents the *ab initio* reconstructed three-dimenional image of the open ^{d}ezrin(T567D) in the PIP_2·^{d}ezrin(T567D)·F-actin complex, which adopts an elongated spiral shape. These results also show that PIP_2 is required for ezrin to bind to F-actin.

At the contrast points other than 40% D_2O, the hydrogenated F-actin filament contributes to scattering (Fig. 7*A*). The scattering from the F-actin filament or from the PIP2·^{d}ezrin(T567D)·F-actin complex can be considered as that from long rod-like structures with random orientations. Analyzing the small angle scattering data $QI(Q)$ of such rod-like structures typically yields structural information about the cross-section of the filament complex (60, 71). The cross-section length distribution function $P_c(r)$ of the PIP_2·^{d}ezrin(T567D)·F-actin complex are shown in Fig. 7*B* at three contrasts of 0, 20, and 100% D_2O.

In 100% D_2O, $P_c(r)$ of the PIP_2·^{d}ezrin(T567D)·F-actin complex is similar to that of F-actin alone and to the computed $P_c(r)$ of an F-actin model (see Fig. 7*D*). The PIP_2·^{d}ezrin(T567D)·F-actin complex has similar cross-section maximum dimension ($D_{c,\,max}$) and cross-section radius of gyration (R_c) as the F-actin filament (Table 2). This result suggests that the scattering comes mainly from the F-actin filament in 100% D_2O.

In 0 and 20% D_2O, $P_c(r)$ ratios of the PIP_2·^{d}ezrin(T567D)·F-actin complex have $D_{c,\,max}$ = 130 Å, and the cross-section center-of-mass distance between F-actin and ^{d}ezrin(T567D) is about 100 Å (Fig. 7*B*), which is less than half the length of the fully opened ezrin. This comparison suggests that the opened ezrin does not bind to the F-actin filament vertically with only the C-ERMAD domain in contact with actin. Our SPR experi-

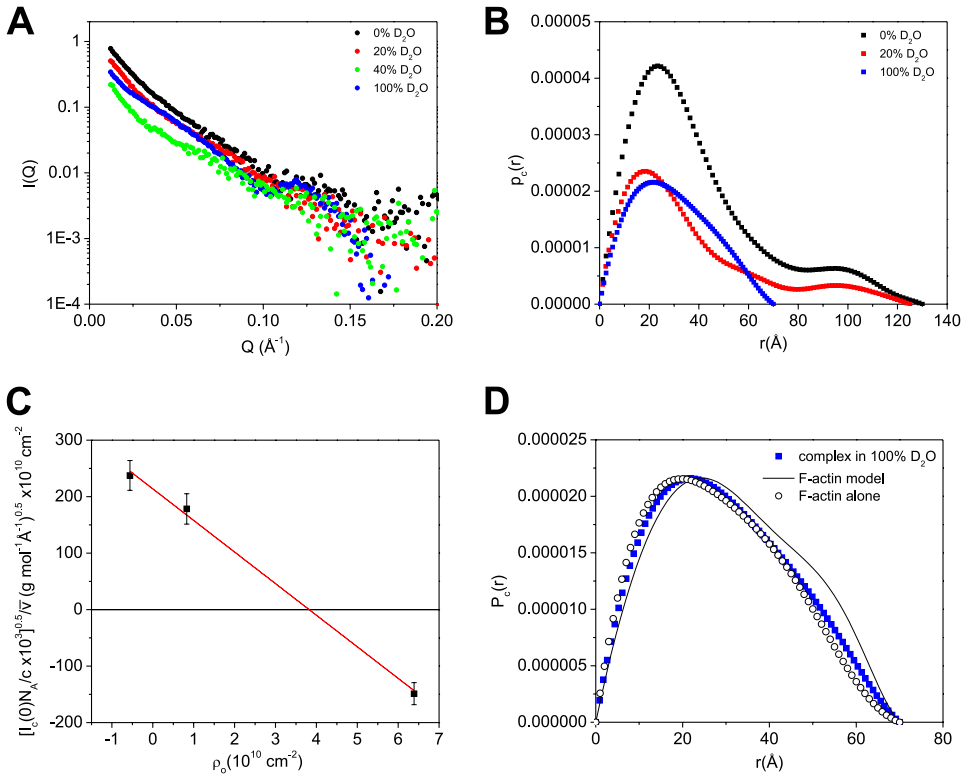

FIGURE 7. **Cross-section analysis of the PIP_2·^{d}ezrin(T567D)·F-actin complex.** *A,* SANS *I*(*Q*) of the PIP_2·^{d}ezrin(T567D)·F-actin complex in 0, 20, 40, and 100% D_2O buffer. *B,* $P_c(r)$ of the complex in 0, 20, and 100% D_2O. *C,* M_L of the PIP_2·^{d}ezrin(T567D)·F-actin is obtained from the slope of normalized $I(0)^{0.5}$ *versus* ρ_o plot (see supplemental Equation S2. In supplemental Equation S2, the hydrogen/deuterium exchange of labile protons, which depends on the kinetics of hydrogen/deuterium exchange of proteins, is not considered. *D,* comparing $P_c(r)$ of F-actin alone (*open black circle*) and that of PIP_2·^{d}ezrin(T567D)·F-actin complex (*filled blue square*) in 100% D_2O. The line is the $P_c(r)$ value computed from an F-actin model composed of 20 actin monomers using Protein Data Bank 3B5U as the starting structure (93).

ments find that FERM binds to F-actin with high affinity (supplemental Fig. S6*A*), in agreement with previous reports (32, 72). In addition, we find that the helical linker region of ezrin also binds to F-actin (supplemental Fig. S6*B*). Based on the open structure of ^{d}ezrin(T567D), the cross-section structure of the PIP_2·^{d}ezrin(T567D)·F-actin complex, and the SPR binding results, we propose a model that the opened ezrin binds longitudinally along the F-actin filament (see Fig. 8*A*). In this model, ezrin interacts with F-actin more extensively beside the putative C-ERMAD.

Using the SANS data in 0 and 20% D_2O as a constraint, we have performed rigid-body modeling. The rigid-body modeling docks the open form ezrin (from Fig. 7*C*) to a 20-mer F-actin with different orientations. The results indicate that the model shown in Fig. 8*A* fits best the SANS data in 0 and 20% D2O. Alternative models that do not fit the SANS data as well are shown in Fig. 9.

Fig. 7*C* shows the normalized cross-section forward scattering as a function of scattering length density of the buffer background. The square root of the slope gives the mass per unit length (M_L) of the complex (see supplemental material). The M_L of complex is listed in Table 2, together with that of F-actin filament. A Stuhrmann plot of the cross-section radius of gyration R_{gc}^2 against the contrast $1/\Delta\rho$ does not give a straight line, indicating that the distribution of ^{d}ezrin(T567D) and PIP_2 around the hydrogenated F-actin filament is not symmetric.

In addition, we have also performed SANS on ^{d}ezrin(S249D/T567D) that is incubated simultaneously with hydrogenated scaffolding protein NHERF1 and with F-actin. SPR binding experiments indicate that, compared with the wild-type ezrin, a considerable fraction of this double mutant ezrin(S249D/T567D) is capable of binding to NHERF1 (supplemental Table S2). We thus posit that incubating ^{d}ezrin(S249D/T567D) with both NHERF1 and F-actin may trap and stabilize the open structure. SANS was performed on the incubation that contains 28.9 μM hydrogenated NHERF1, 28.9 μM deuterated ^{d}ezrin(S249D/T567D), and 124.4 μM hydrogenated F-actin in 0, 40, and 100% D_2O buffer.

In 40% D_2O, in which both NHERF1 and F-actin are invisible, ^{d}ezrin(S249D/T567D) undergoes large conformational changes when compared with the closed form in solution, with R_g increases to 64.2 ± 1.5 Å, and D_{max} expands to 240 ± 5 Å (supplemental Fig. S7 and Table 1). The reconstructed three-dimenional shape of ^{d}ezrin(S249D/T567D) adopts an L-shaped open structure (supplemental Fig. S8*C*). When incubating ^{d}ezrin(S249D/T567D) with NHERF1 alone at a 1:1 molar ratio, we find that ^{d}ezrin(S249D/T567D) does not have apparent conformational changes using contrast-matching SANS. Thus, ^{d}ezrin(S249D/T567D) requires the FERM domain to be occupied by NHERF1 and F-actin simultaneously to adopt an open structure.

In 40% D_2O, the overall size of open ^{d}ezrin(S249D/T567D) in the NHERF1·^{d}ezrin(S249D/T567D)·F-actin complex is smaller than ^{d}ezrin(T567D) in the PIP_2·^{d}ezrin(T567D)·F-actin complex (see Table 1). The larger size of ^{d}ezrin(T567D) in complex with PIP_2 and F-actin is probably due to the scattering from the PIP_2

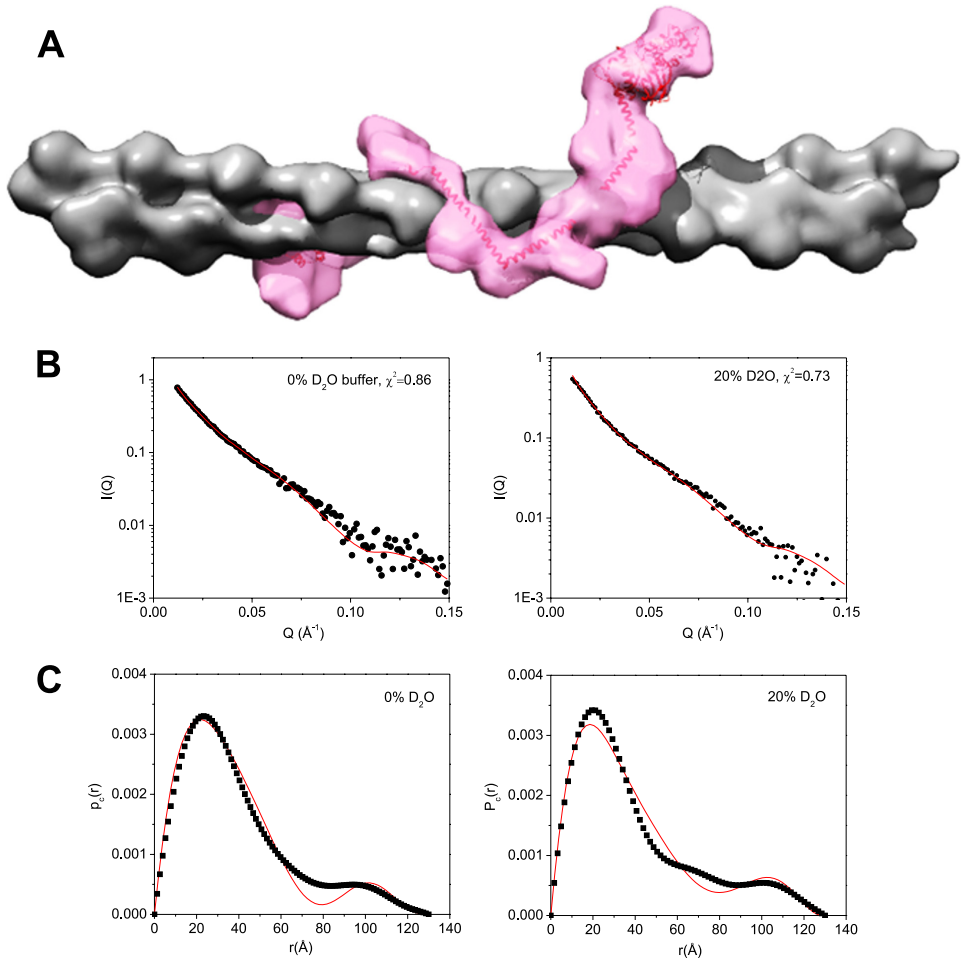

FIGURE 8. *A,* model of ezrin(T567D) bound to F-actin obtained using SANS data as constraint. The open structure of ^{d}ezrin(T567D) is taken from Fig. 6*C*. *B,* fitting of *I*(*Q*) computed from the model shown in *A* to the experimental SANS *I*(*Q*) from the PIP_2·^{d}ezrin(T567D)·F-actin in 0 and 10% D_2O buffer. *C,* comparing $P_c(r)$ value computed from the model shown in *A* and that from the experimental data in 0 and 20% D_2O buffer. The goodness of fit value of χ^2 is shown on the graph.

molecules bound to ^{d}ezrin(T567D). Alternatively, PIP_2 is more capable of extending ezrin(T567D) and stabilizing the open conformation on F-actin than NHERF1. In 0% D_2O, all three components of the NHERF1·^{d}ezrin(S249D/T567D)·F-actin complex are visible to neutrons; $P_c(r)$ of the complex has a $D_{c,\,max}$ of 110 Å and an extra peak at about 100 Å as compared with F-actin filament alone (supplemental Fig. S9*A*). In 100% D_2O in which ^{d}ezrin(S249D/T567D) is invisible and only the hydrogenated NHERF1 and F-actin scatter neutrons, $P_c(r)$ of the complex also has a peak at about 100 Å (supplemental Fig. S9*A*). This peak is due to the contribution from NHERF1, and the maximum of the second peak in $P_c(r)$ indicates that the cross-section center-of-mass distance between the F-actin filament and NHERF1 is about 95 Å. Because the full-length of an open ezrin is about 240–300 Å in the NHERF1·^{d}ezrin(S249D/T567D)·F-actin, the short cross-section center-of-mass distance between NHERF1 and F-actin can only implicate that the extended ^{d}ezrin(S249D/T567D) binds intimately in the F-actin filament, forming extensive contacts with F-actin besides the canonical C-ERMAD (supplemental Fig. S9*B*).

To summarize, binding of ezrin to F-actin requires either PIP_2 or NHERF1 to be bound to the FERM domain of ezrin. Once bound to F-actin, ezrin does not stand perpendicular on the F-actin filament with only the C-ERMAD domain in contact with F-actin, as often depicted in the published cartoon pictures. Instead, our model shows that once bound to F-actin, ezrin forms extensive contacts with F-actin.

DISCUSSION

We have determined the structural changes of the full-length ezrin upon binding to PIP_2 and to F-actin using contrast variation SANS. Using gel filtration, we show that the conformational opening of ezrin in response to PIP_2 binding is cooperative, but the cooperativity is disrupted by the phospho-mimetic mutation S249D in the FERM domain. Using SPR, we find that the S249D mutation weakens the binding affinity of FERM domain for PIP_2 and changes the kinetics of FERM to PIP_2 binding. Furthermore, our study indicates that ezrin binding to F-actin requires the simultaneous binding of ezrin to either PIP_2 or in the case of the double mutant ezrin(S249D/T567D) to the scaffolding protein NHERF1. According to cross-section analysis of the SANS data, the cross-section center-of-mass distance between F-actin and the bound ezrin is significantly shorter than the full length of the activated ezrin, suggesting that the opened ezrin is collapsed on F-actin and forms extensive contact with the fila-

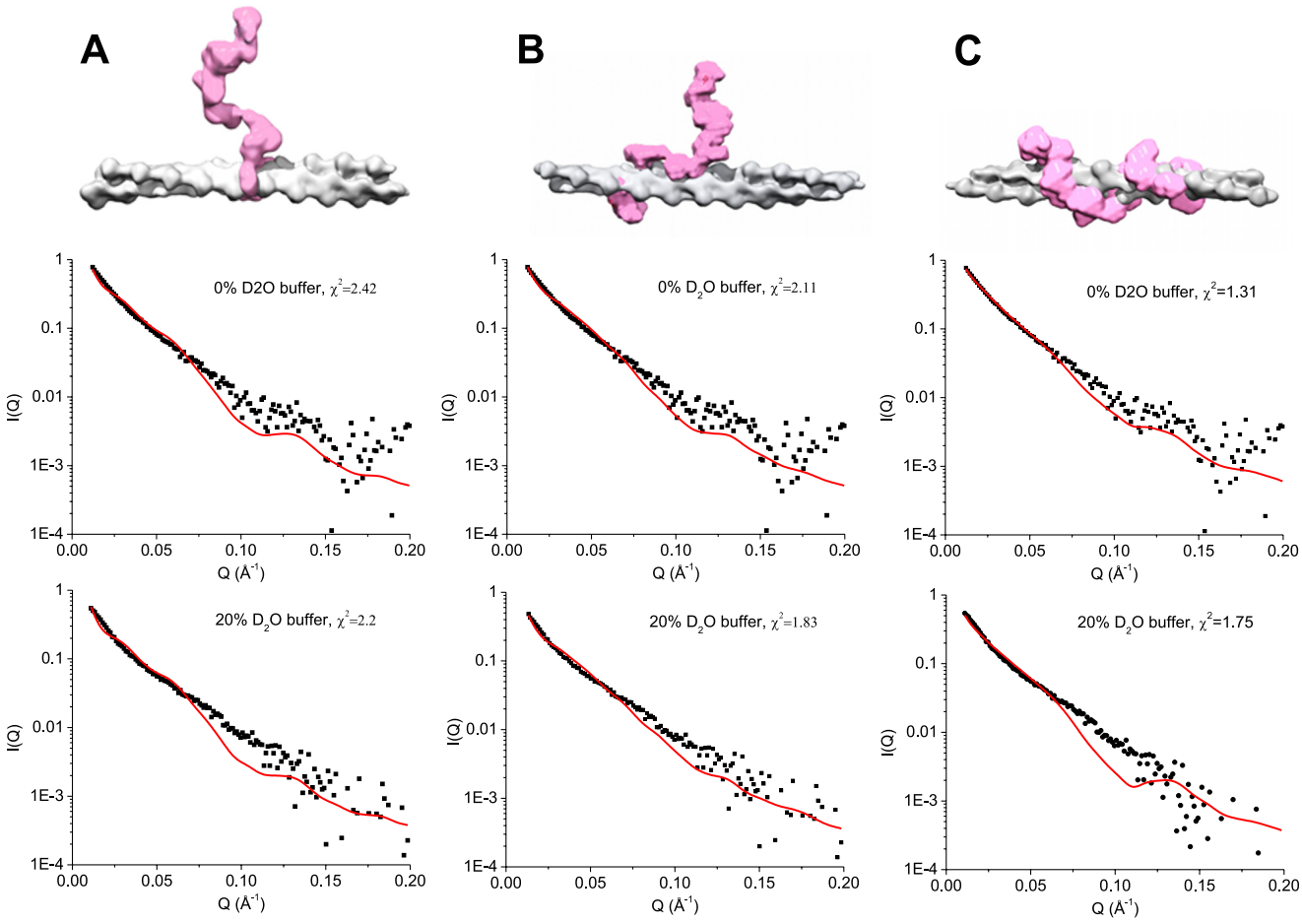

FIGURE 9. **Alternative models of ezrin binding to F-actin show worse fit to the experimental SANS data than the model presented in Fig. 8.**

ment. This model of the ezrin/F-actin interaction is thus different from that generally depicted in the published literature, in which the activated ezrin binds vertically with only the C-ERMAD in contact with F-actin.

We find that the opening of ezrin or ezrin(T567D) in response to PIP_2 binding is cooperative. Cooperative binding warrants a robust regulation of a biochemical process in response to a ligand or an effector molecule. A cooperative regulation of ezrin activation by PIP_2 may suggest the need for acute spatial-temporal regulation of ezrin functions in the cellular context. Although PIP_2 includes only about 0.5–1% of the cell membrane phospholipids, PIP_2 is highly localized in a variety of subcellular compartments and microdomains due to local synthesis and sequestering of PIP_2 (73–75). PIP_2 is particularly localized in the apical membrane of epithelial cells, in lamellipodia, in microvilli, and at the cell junctions, in which ezrin plays important roles in assembling and maintaining these specialized subcellular structures (14, 76–79). An effective spatial-temporal regulation of the assembly and disassembly of the protein complexes is required for the dynamic turnover of these subcellular structures. As a result of cooperative activation of ezrin by PIP_2, PIP_2 and ezrin may contribute significantly to the dynamics of these specialized subcellular structures. Also, there is increasing evidence that the activated ezrin binds to target proteins that trigger the subsequent propagation of downstream allosteric binding signals in the membrane cytoskeleton (15, 80, 81). For instance, ezrin activates NHERF1 and induces long range allostery in NHERF1 so as to strengthen the interactions of NHERF1 with transmembrane proteins and other signaling proteins (24, 27, 70). In turn, NHERF1 also allosterically activates other proteins, such as the scaffolding protein PDZK1 that binds to downstream targets for the assembly microvillus structures on the cell surface (15, 81). Ezrin is a crucial player in protein dynamics, long range allostery, and signal transduction (70, 82).

Altering the subtle cooperativity of ezrin activation in response to PIP_2 binding could have substantial impact on cellular functions. Indeed, we find that ezrin phosphorylated at Ser-249 or the ezrin(S249D) mutant is no longer localized in the apical membrane or at the cell-cell junctions in polarized epithelial cells as the wild-type ezrin, but it is largely degraded or forms clustered aggregates in the cytoplasm. Cells expressing the ezrin(S249D) mutant show altered morphology and weakened cell-cell adhesion as compared with cells expressing the wild-type ezrin. Furthermore, the localization of adherens junction marker proteins, E-cadherin and α-catenin, are diffuse and reduced at the cell-cell junctions in cells expressing ezrin(S249D) mutants. It remains to be determined if other phosphorylation sites, such as Tyr-

145 (83), in the FERM domain can influence the PIP_2 binding behavior.

The S249D mutation affects both the affinity and kinetic rate constants of FERM to PIP_2 binding, even though this Ser-249 is outside the two patches of positively charged residues that are necessary for FERM binding to PIP_2 (35, 38, 84). Thus, mutating the Ser-249 to the negatively charged Asp may affect the long range electrostatic field on the surface of the FERM domain. Electrostatic interactions are likely to be the basis of FERM to PIP_2 binding, which are found in many other protein domains that bind to phosphoinositide lipids with limited structural specificity (74, 85).

Without PIP_2, the phospho-mimic mutants adopt essentially closed conformation in solution as the autoinhibited wild-type ezrin. However, a considerable fraction of the phospho-mimetics is active and capable of binding to NHERF1 when compared with the wild-type protein. It is likely that the phospho-mimetic mutants are more dynamic so that a small fraction of the mutants is open for a period of time and becomes competent to bind to NHERF. The SANS results on the T567D mutant provide an alternative view from a previous electron microscopy study that finds this mutant to be completely open (86). This is because SANS samples an ensemble of molecules, whereas EM selectively looks at a particular population of molecules. A small fraction of activated and open ezrin(T567D) may not contribute significantly to the ensemble averaged R_g and D_{max} values measured by SANS. It would be interesting to determine the kinetics and dynamics of ezrin opening in future studies (87).

Our results show that ezrin binding to F-actin requires the simultaneous binding of ezrin to either PIP_2 or to the scaffolding protein NHERF1. Furthermore, the neutron scattering cross-section analyses of both the PIP_2·^{d}ezrin(T567D)·F-actin and the NHERF1·^{d}ezrin(S249D/T567D)·F-actin complexes suggest that the opened ezrin does not stand vertically on the F-actin filament. Instead, we propose a model that ezrin collapses on F-actin forming extensive contacts. Previous studies (32) and our own binding experiment show that the FERM domain has the capability to interact with F-actin strongly. The FERM domain is likely to also bind F-actin and is anchored in the actin filament.

Our structural model of a collapsed ezrin spans about 10 actin monomers on the F-actin filament. This model corroborates the findings from previous biochemical studies that ezrin binding to actin is saturable with a 1:8–10 molar ratio (32, 88). The model we presented here indicates that ezrin acts a spatial ruler on the F-actin filament.

In cells, through extensive contacts with F-actin, ezrin can bring the cell membrane close to the underlying F-actin cytoskeletal network. Indeed, an electron tomography study of the membrane skeleton reveals that the actin filaments are closely associated with the cytoplasmic surface of the plasma membrane within 10.2 nm (89). Ezrin and NHERF1 are distributed along almost the entire microvillus structure (14). The growing F-actin filaments can have intimate interactions with the lipid membrane and support the expanding cell membrane. In this scenario, ezrin may play active roles in regulating the adhesion and tension between the membrane and the cytoskeleton, as required for forming many subcellular structures and for regulating many transmembrane proteins at the cell surface (16, 90–92).

Acknowledgments—City College of New York was recipient of National Institutes of Health Grant 2G12 RR003060 from the NCRR. The work performed at Oak Ridge National Laboratory was supported by the Division of Scientific User Facilities, Department of Energy Basic Energy Sciences, and the Oak Ridge National Laboratory Directed Research and Development Program. We thank D. M. Engelman for comments on the manuscript.

REFERENCES

1. Bretscher, A., Edwards, K., and Fehon, R. G. (2002) ERM proteins and merlin. Integrators at the cell cortex. *Nat. Rev. Mol. Cell Biol.* **3,** 586–599
2. Fehon, R. G., McClatchey, A. I., and Bretscher, A. (2010) Organizing the cell cortex. The role of ERM proteins. *Nat. Rev. Mol. Cell Biol.* **11,** 276–287
3. Roumier, A., Olivo-Marin, J. C., Arpin, M., Michel, F., Martin, M., Mangeat, P., Acuto, O., Dautry-Varsat, A., and Alcover, A. (2001) The membrane-microfilament linker ezrin is involved in the formation of the immunological synapse and in T cell activation. *Immunity* **15,** 715–728
4. Arpin, M., Chirivino, D., Naba, A., and Zwaenepoel, I. (2011) Emerging role for ERM proteins in cell adhesion and migration. *Cell Adh. Migr.* **5,** 199–206
5. McClatchey, A. I., and Fehon, R. G. (2009) Merlin and the ERM proteins. Regulators of receptor distribution and signaling at the cell cortex. *Trends Cell Biol.* **19,** 198–206
6. Casaletto, J. B., Saotome, I., Curto, M., and McClatchey, A. I. (2011) Ezrin-mediated apical integrity is required for intestinal homeostasis. *Proc. Natl. Acad. Sci. U.S.A.* **108,** 11924–11929
7. Saotome, I., Curto, M., and McClatchey, A. I. (2004) Ezrin is essential for epithelial organization and villus morphogenesis in the developing intestine. *Dev. Cell* **6,** 855–864
8. Louvet-Vallée, S. (2000) ERM proteins. From cellular architecture to cell signaling. *Biol. Cell* **92,** 305–316
9. McClatchey, A. I. (2003) Merlin and ERM proteins. Unappreciated roles in cancer development? *Nat. Rev. Cancer* **3,** 877–883
10. Yu, Y., Khan, J., Khanna, C., Helman, L., Meltzer, P. S., and Merlino, G. (2004) Expression profiling identifies the cytoskeletal organizer ezrin and the developmental homeoprotein Six-1 as key metastatic regulators. *Nat. Med.* **10,** 175–181
11. Khanna, C., Wan, X., Bose, S., Cassaday, R., Olomu, O., Mendoza, A., Yeung, C., Gorlick, R., Hewitt, S. M., and Helman, L. J. (2004) The membrane-cytoskeleton linker ezrin is necessary for osteosarcoma metastasis. *Nat. Med.* **10,** 182–186
12. Pujuguet, P., Del Maestro, L., Gautreau, A., Louvard, D., and Arpin, M. (2003) Ezrin regulates E-cadherin-dependent adherens junction assembly through Rac1 activation. *Mol. Biol. Cell* **14,** 2181–2191
13. Prag, S., Parsons, M., Keppler, M. D., Ameer-Beg, S. M., Barber, P., Hunt, J., Beavil, A. J., Calvert, R., Arpin, M., Vojnovic, B., and Ng, T. (2007) Activated ezrin promotes cell migration through recruitment of the GEF Dbl to lipid rafts and preferential downstream activation of Cdc42. *Mol. Biol. Cell* **18,** 2935–2948
14. Hanono, A., Garbett, D., Reczek, D., Chambers, D. N., and Bretscher, A. (2006) EPI64 regulates microvillar subdomains and structure. *J. Cell Biol.* **175,** 803–813
15. LaLonde, D. P., Garbett, D., and Bretscher, A. (2010) A regulated complex of the scaffolding proteins PDZK1 and EBP50 with ezrin contribute to microvillar organization. *Mol. Biol. Cell* **21,** 1519–1529
16. Charras, G. T., Hu, C. K., Coughlin, M., and Mitchison, T. J. (2006) Reassembly of contractile actin cortex in cell blebs. *J. Cell Biol.* **175,** 477–490
17. Wong, W., and Gough, N. R. (2009) Focus issue. The protein dynamics of cell signaling. *Sci. Signal.* **2,** eg4
18. Liu, Y., Belkina, N. V., and Shaw, S. (2009) HIV infection of T cells. Actin-in and actin-out. *Sci. Signal.* **2,** pe23

19. Yonemura, S., Hirao, M., Doi, Y., Takahashi, N., Kondo, T., Tsukita, S., and Tsukita, S. (1998) Ezrin/radixin/moesin (ERM) proteins bind to a positively charged amino acid cluster in the juxta-membrane cytoplasmic domain of CD44, CD43, and ICAM-2. *J. Cell Biol.* **140,** 885–895
20. Mahon, M. J. (2009) The parathyroid hormone 1 receptor directly binds to the FERM domain of ezrin, an interaction that supports apical receptor localization and signaling in LLC-PK1 cells. *Mol. Endocrinol.* **23,** 1691–1701
21. Ardura, J. A., Wang, B., Watkins, S. C., Vilardaga, J. P., and Friedman, P. A. (2011) Dynamic Na^+-H^+ exchanger regulatory factor-1 association and dissociation regulate parathyroid hormone receptor trafficking at membrane microdomains. *J. Biol. Chem.* **286,** 35020–35029
22. Reczek, D., Berryman, M., and Bretscher, A. (1997) Identification of EBP50. A PDZ-containing phosphoprotein that associates with members of the ezrin-radixin-moesin family. *J. Cell Biol.* **139,** 169–179
23. Yun, C. H., Oh, S., Zizak, M., Steplock, D., Tsao, S., Tse, C. M., Weinman, E. J., and Donowitz, M. (1997) cAMP-mediated inhibition of the epithelial brush border Na^+/H^+ exchanger, NHE3, requires an associated regulatory protein. *Proc. Natl. Acad. Sci. U.S.A.* **94,** 3010–3015
24. Li, J., Dai, Z., Jana, D., Callaway, D. J., and Bu, Z. (2005) Ezrin controls the macromolecular complexes formed between an adapter protein Na^+/H^+ exchanger regulatory factor and the cystic fibrosis transmembrane conductance regulator. *J. Biol. Chem.* **280,** 37634–37643
25. Hall, R. A., Ostedgaard, L. S., Premont, R. T., Blitzer, J. T., Rahman, N., Welsh, M. J., and Lefkowitz, R. J. (1998) A C-terminal motif found in the β_2-adrenergic receptor, P2Y1 receptor, and cystic fibrosis transmembrane conductance regulator determines binding to the Na^+/H^+ exchanger regulatory factor family of PDZ proteins. *Proc. Natl. Acad. Sci. U.S.A.* **95,** 8496–8501
26. Weinman, E. J., Hall, R. A., Friedman, P. A., Liu-Chen, L. Y., and Shenolikar, S. (2006) The association of NHERF adaptor proteins with G protein-coupled receptors and receptor tyrosine kinases. *Annu. Rev. Physiol.* **68,** 491–505
27. Li, J., Callaway, D. J., and Bu, Z. (2009) Ezrin induces long range interdomain allostery in the scaffolding protein NHERF1. *J. Mol. Biol.* **392,** 166–180
28. Li, J., Poulikakos, P. I., Dai, Z., Testa, J. R., Callaway, D. J., and Bu, Z. (2007) Protein kinase C phosphorylation disrupts Na^+/H^+ exchanger regulatory factor 1 autoinhibition and promotes cystic fibrosis transmembrane conductance regulator macromolecular assembly. *J. Biol. Chem.* **282,** 27086–27099
29. Turunen, O., Wahlström, T., and Vaheri, A. (1994) Ezrin has a COOH-terminal actin-binding site that is conserved in the ezrin protein family. *J. Cell Biol.* **126,** 1445–1453
30. Gary, R., and Bretscher, A. (1995) Ezrin self-association involves binding of an N-terminal domain to a normally masked C-terminal domain that includes the F-actin binding site. *Mol. Biol. Cell* **6,** 1061–1075
31. Pestonjamasp, K., Amieva, M. R., Strassel, C. P., Nauseef, W. M., Furthmayr, H., and Luna, E. J. (1995) Moesin, ezrin, and p205 are actin-binding proteins associated with neutrophil plasma membranes. *Mol. Biol. Cell* **6,** 247–259
32. Roy, C., Martin, M., and Mangeat, P. (1997) A dual involvement of the amino-terminal domain of ezrin in F- and G-actin binding. *J. Biol. Chem.* **272,** 20088–20095
33. Li, Q., Nance, M. R., Kulikauskas, R., Nyberg, K., Fehon, R., Karplus, P. A., Bretscher, A., and Tesmer, J. J. (2007) Self-masking in an intact ERM-merlin protein. An active role for the central α-helical domain. *J. Mol. Biol.* **365,** 1446–1459
34. Smith, W. J., Nassar, N., Bretscher, A., Cerione, R. A., and Karplus, P. A. (2003) Structure of the active N-terminal domain of ezrin. Conformational and mobility changes identify keystone interactions. *J. Biol. Chem.* **278,** 4949–4956
35. Hamada, K., Shimizu, T., Matsui, T., Tsukita, S., and Hakoshima, T. (2000) Structural basis of the membrane-targeting and unmasking mechanisms of the radixin FERM domain. *EMBO J.* **19,** 4449–4462
36. Pearson, M. A., Reczek, D., Bretscher, A., and Karplus, P. A. (2000) Structure of the ERM protein moesin reveals the FERM domain fold masked by an extended actin binding tail domain. *Cell* **101,** 259–270
37. Niggli, V., Andréoli, C., Roy, C., and Mangeat, P. (1995) Identification of a phosphatidylinositol 4,5-bisphosphate-binding domain in the N-terminal region of ezrin. *FEBS Lett.* **376,** 172–176
38. Barret, C., Roy, C., Montcourrier, P., Mangeat, P., and Niggli, V. (2000) Mutagenesis of the phosphatidylinositol 4,5-bisphosphate (PIP_2)-binding site in the NH_2-terminal domain of ezrin correlates with its altered cellular distribution. *J. Cell Biol.* **151,** 1067–1080
39. Hirao, M., Sato, N., Kondo, T., Yonemura, S., Monden, M., Sasaki, T., Takai, Y., and Tsukita, S. (1996) Regulation mechanism of ERM (ezrin/radixin/moesin) protein/plasma membrane association. Possible involvement of phosphatidylinositol turnover and Rho-dependent signaling pathway. *J. Cell Biol.* **135,** 37–51
40. Nakamura, F., Huang, L., Pestonjamasp, K., Luna, E. J., and Furthmayr, H. (1999) Regulation of F-actin binding to platelet moesin *in vitro* by both phosphorylation of threonine 558 and polyphosphatidylinositides. *Mol. Biol. Cell* **10,** 2669–2685
41. Matsui, T., Maeda, M., Doi, Y., Yonemura, S., Amano, M., Kaibuchi, K., and Tsukita, S. (1998) Rho-kinase phosphorylates COOH-terminal threonines of ezrin/radixin/moesin (ERM) proteins and regulates their head-to-tail association. *J. Cell Biol.* **140,** 647–657
42. Wald, F. A., Oriolo, A. S., Mashukova, A., Fregien, N. L., Langshaw, A. H., and Salas, P. J. (2008) Atypical protein kinase Cι activates ezrin in the apical domain of intestinal epithelial cells. *J. Cell Sci.* **121,** 644–654
43. Belkina, N. V., Liu, Y., Hao, J. J., Karasuyama, H., and Shaw, S. (2009) LOK is a major ERM kinase in resting lymphocytes and regulates cytoskeletal rearrangement through ERM phosphorylation. *Proc. Natl. Acad. Sci. U.S.A.* **106,** 4707–4712
44. ten Klooster, J. P., Jansen, M., Yuan, J., Oorschot, V., Begthel, H., Di Giacomo, V., Colland, F., de Koning, J., Maurice, M. M., Hornbeck, P., and Clevers, H. (2009) Mst4 and ezrin induce brush borders downstream of the Lkb1/Strad/Mo25 polarization complex. *Dev. Cell* **16,** 551–562
45. Oshiro, N., Fukata, Y., and Kaibuchi, K. (1998) Phosphorylation of moesin by Rho-associated kinase (Rho-kinase) plays a crucial role in the formation of microvilli-like structures. *J. Biol. Chem.* **273,** 34663–34666
46. Yonemura, S., Tsukita, S., and Tsukita, S. (1999) Direct involvement of ezrin/radixin/moesin (ERM)-binding membrane proteins in the organization of microvilli in collaboration with activated ERM proteins. *J. Cell Biol.* **145,** 1497–1509
47. Gautreau, A., Louvard, D., and Arpin, M. (2000) Morphogenic effects of ezrin require a phosphorylation-induced transition from oligomers to monomers at the plasma membrane. *J. Cell Biol.* **150,** 193–203
48. Fievet, B. T., Gautreau, A., Roy, C., Del Maestro, L., Mangeat, P., Louvard, D., and Arpin, M. (2004) Phosphoinositide binding and phosphorylation act sequentially in the activation mechanism of ezrin. *J. Cell Biol.* **164,** 653–659
49. Bu, Z. M., Perlo, A., Johnson, G. E., Olack, G., Engelman, D. M., and Wyckoff, H. W. (1998) A small angle x-ray scattering apparatus for studying biological macromolecules in solution. *J. Appl. Crystallogr.* **31,** 533–543
50. Bu, Z., and Engelman, D. M. (1999) A method for determining transmembrane helix association and orientation in detergent micelles using small angle x-ray scattering. *Biophys. J.* **77,** 1064–1073
51. Ho, D. L., Byrnes, W. M., Ma, W. P., Shi, Y., Callaway, D. J., and Bu, Z. (2004) Structure-specific DNA-induced conformational changes in Taq polymerase revealed by small angle neutron scattering. *J. Biol. Chem.* **279,** 39146–39154
52. Zhao, J. K., Gao, C. Y., and Liu, D. (2010) *J. Appl. Crystallogr.* **43,** 1068–1077
53. Zhao, J. K. (2011) Nuclear instruments and methods in physics research section A. Accelerators spectrometers detectors and associated equipment **647,** 107–111
54. Wignall, G. D., and Bates, F. S. (1987) Absolute calibration of small angle neutron scattering data. *J. Appl. Crystallogr.* **20,** 28–40
55. Semenyuk, A. V., and Svergun, D. I. (1991) GNOM. A program package for small angle scattering data processing. *J. Appl. Crystallogr.* **24,** 537–540
56. Svergun, D. I. (1999) Restoring low resolution structure of biological macromolecules from solution scattering using simulated annealing. *Biophys. J.* **76,** 2879–2886

57. Volkov, V. V., and Svergun, D. I. (2003) Uniqueness of *ab initio* shape determination in small angle scattering. *J. Appl. Crystallogr.* **36,** 860–864
58. Wriggers, W., and Chacón, P. (2001) Using Situs for the registration of protein structures with low resolution bead models from x-ray solution scattering. *J. Appl. Crystallogr.* **34,** 773–776
59. Pettersen, E. F., Goddard, T. D., Huang, C. C., Couch, G. S., Greenblatt, D. M., Meng, E. C., and Ferrin, T. E. (2004) UCSF Chimera. A visualization system for exploratory research and analysis. *J. Comput. Chem.* **25,** 1605–1612
60. Whitten, A. E., Jeffries, C. M., Harris, S. P., and Trewhella, J. (2008) Cardiac myosin-binding protein C decorates F-actin. Implications for cardiac function. *Proc. Natl. Acad. Sci. U.S.A.* **105,** 18360–18365
61. Orthaber, D., Bergmann, A., and Glatter, O. (2000) SAXS experiments on absolute scale with Kratky systems using water as a secondary standard. *J. Appl. Crystallogr.* **33,** 218–225
62. Jacrot, B., and Zaccai, G. (1981) Determination of molecular weight by neutron scattering. *Biopolymers* **20,** 2413–2426
63. Dard, N., Louvet-Vallée, S., Santa-Maria, A., and Maro, B. (2004) Phosphorylation of ezrin on threonine 567 plays a crucial role during compaction in the mouse early embryo. *Dev. Biol.* **271,** 87–97
64. Chambers, D. N., and Bretscher, A. (2005) Ezrin mutants affecting dimerization and activation. *Biochemistry* **44,** 3926–3932
65. Finnerty, C. M., Chambers, D., Ingraffea, J., Faber, H. R., Karplus, P. A., and Bretscher, A. (2004) The EBP50-moesin interaction involves a binding site regulated by direct masking on the FERM domain. *J. Cell Sci.* **117,** 1547–1552
66. Terawaki, S., Maesaki, R., and Hakoshima, T. (2006) Structural basis for NHERF recognition by ERM proteins. *Structure* **14,** 777–789
67. Engelman, D. M., and Moore, P. B. (1975) Determination of quaternary structure by small angle neutron scattering. *Annu. Rev. Biophys. Bioeng.* **4,** 219–241
68. Heller, W. T. (2010) Small-angle neutron scattering and contrast variation. A powerful combination for studying biological structures. *Acta Crystallogr. D Biol. Crystallogr.* **66,** 1213–1217
69. Hoeflich, K. P., Tsukita, S., Hicks, L., Kay, C. M., Tsukita, S., and Ikura, M. (2003) Insights into a single rod-like helix in activated radixin required for membrane-cytoskeletal cross-linking. *Biochemistry* **42,** 11634–11641
70. Farago, B., Li, J., Cornilescu, G., Callaway, D. J., and Bu, Z. (2010) Activation of nanoscale allosteric protein domain motion revealed by neutron spin echo spectroscopy. *Biophys. J.* **99,** 3473–3482
71. Glatter, O., and Kratky, O. (eds) (1982) *Small Angle X-ray Scattering,* page 33, Academic Press, New York
72. Mangeat, P., Roy, C., and Martin, M. (1999) ERM proteins in cell adhesion and membrane dynamics. *Trends Cell Biol.* **9,** 187–192
73. McLaughlin, S., Wang, J., Gambhir, A., and Murray, D. (2002) PIP_2 and proteins. Interactions, organization, and information flow. *Annu. Rev. Biophys. Biomol. Struct.* **31,** 151–175
74. Niggli, V. (2005) Regulation of protein activities by phosphoinositide phosphates. *Annu. Rev. Cell Dev. Biol.* **21,** 57–79
75. Di Paolo, G., and De Camilli, P. (2006) Phosphoinositides in cell regulation and membrane dynamics. *Nature* **443,** 651–657
76. Martin-Belmonte, F., Gassama, A., Datta, A., Yu, W., Rescher, U., Gerke, V., and Mostov, K. (2007) PTEN-mediated apical segregation of phosphoinositides controls epithelial morphogenesis through Cdc42. *Cell* **128,** 383–397
77. Lamb, R. F., Ozanne, B. W., Roy, C., McGarry, L., Stipp, C., Mangeat, P., and Jay, D. G. (1997) Essential functions of ezrin in maintenance of cell shape and lamellipodial extension in normal and transformed fibroblasts. *Curr. Biol.* **7,** 682–688
78. Zwaenepoel, I., Naba, A., Da Cunha, M. M., Del Maestro, L., Formstecher, E., Louvard, D., and Arpin, M. (2012) Ezrin regulates microvillus morphogenesis by promoting distinct activities of Eps8 proteins. *Mol. Biol. Cell* **23,** 1080–1094
79. Roch, F., Polesello, C., Roubinet, C., Martin, M., Roy, C., Valenti, P., Carreno, S., Mangeat, P., and Payre, F. (2010) Differential roles of $PtdIns(4,5)P_2$ and phosphorylation in moesin activation during *Drosophila* development. *J. Cell Sci.* **123,** 2058–2067
80. Sneddon, W. B., Syme, C. A., Bisello, A., Magyar, C. E., Rochdi, M. D., Parent, J. L., Weinman, E. J., Abou-Samra, A. B., and Friedman, P. A. (2003) Activation-independent parathyroid hormone receptor internalization is regulated by NHERF1 (EBP50). *J. Biol. Chem.* **278,** 43787–43796
81. LaLonde, D. P., and Bretscher, A. (2009) The scaffold protein PDZK1 undergoes a head-to-tail intramolecular association that negatively regulates its interaction with EBP50. *Biochemistry* **48,** 2261–2271
82. Bu, Z., and Callaway, D. J. (2011) Proteins move! Protein dynamics and long range allostery in cell signaling. *Adv. Protein Chem. Struct. Biol.* **83,** 163–221
83. Srivastava, J., Elliott, B. E., Louvard, D., and Arpin, M. (2005) Src-dependent ezrin phosphorylation in adhesion-mediated signaling. *Mol. Biol. Cell* **16,** 1481–1490
84. Ben-Aissa, K., Patino-Lopez, G., Belkina, N. V., Maniti, O., Rosales, T., Hao, J. J., Kruhlak, M. J., Knutson, J. R., Picart, C., and Shaw, S. (2012) Activation of moesin, a protein that links actin cytoskeleton to the plasma membrane, occurs by phosphatidylinositol 4,5-bisphosphate (PIP_2) binding sequentially to two sites and releasing an autoinhibitory linker. *J. Biol. Chem.* **287,** 16311–16323
85. Moravcevic, K., Oxley, C. L., and Lemmon, M. A. (2012) Conditional peripheral membrane proteins. Facing up to limited specificity. *Structure* **20,** 15–27
86. Ishikawa, H., Tamura, A., Matsui, T., Sasaki, H., Hakoshima, T., Tsukita, S., and Tsukita, S. (2001) Structural conversion between open and closed forms of radixin. Low angle shadowing electron microscopy. *J. Mol. Biol.* **310,** 973–978
87. Bu, Z., Biehl, R., Monkenbusch, M., Richter, D., and Callaway, D. J. (2005) Coupled protein domain motion in Taq polymerase revealed by neutron spin-echo spectroscopy. *Proc. Natl. Acad. Sci. U.S.A.* **102,** 17646–17651
88. Yao, X., Cheng, L., and Forte, J. G. (1996) Biochemical characterization of ezrin-actin interaction. *J. Biol. Chem.* **271,** 7224–7229
89. Morone, N., Fujiwara, T., Murase, K., Kasai, R. S., Ike, H., Yuasa, S., Usukura, J., and Kusumi, A. (2006) Three-dimensional reconstruction of the membrane skeleton at the plasma membrane interface by electron tomography. *J. Cell Biol.* **174,** 851–862
90. Sheetz, M. P., Sable, J. E., and Döbereiner, H. G. (2006) Continuous membrane-cytoskeleton adhesion requires continuous accommodation to lipid and cytoskeleton dynamics. *Annu. Rev. Biophys. Biomol. Struct.* **35,** 417–434
91. Zhu, L., Hatakeyama, J., Chen, C., Shastri, A., Poon, K., and Forte, J. G. (2008) Comparative study of ezrin phosphorylation among different tissues. More is good; too much is bad
92. Alexander, R. T., Furuya, W., Szászi, K., Orlowski, J., and Grinstein, S. (2005) Rho GTPases dictate the mobility of the Na/H exchanger NHE3 in epithelia. Role in apical retention and targeting. *Proc. Natl. Acad. Sci. U.S.A.* **102,** 12253–12258
93. Cong, Y., Topf, M., Sali, A., Matsudaira, P., Dougherty, M., Chiu, W., and Schmid, M. F. (2008) Crystallographic conformers of actin in a biologically active bundle of filaments. *J. Mol. Biol.* **375,** 331–336